IEEE Robotics and Automation Letters (RA-L) paper, presented at ICRA 2024, Yokohama, Japan. Cite as RA-L paper.

Human Gait Cost Function Varies with Walking Speed: an Inverse Optimal Control Study

Jiacheng Weng, Ehsan Hashemi, *Senior Member, IEEE*, and Arash Arami, *Member, IEEE*

***Abstract*—This work investigates the optimal cost function composition for human gait at different walking speeds. Kinematic and kinetic data for walking at four walking speeds were collected from five able-bodied individuals. The data was then used to recover optimal cost functions in a predictive simulation environment with musculoskeletal models. 20 inverse optimal control (IOC) problems were solved for cost function weight tuning using the previously developed and validated Adaptive Reference IOC (AR-IOC) algorithm. Given the walking speed range examined (0.6-1.5m/s), the converged cost function weights suggest that the increase in walking speed attributes to a reduction of foot sliding penalty weight and weight increase for the center of mass (CoM) acceleration and stability as confirmed by several experiments. Furthermore, we did not observe any significant weight shift in effort reduction between the upper and the lower body with respect to walking speed. The obtained results from this study can be used in a toolbox for obtaining subject- and task-specific cost functions and assisting the development of personalized rehabilitation technologies.**

***Index Terms*—Inverse optimal control, predictive simulation, rehabilitation, walking, gait**

I. Introduction

Human movement studies have improved our understanding of the complex interaction among the central nervous system (CNS), musculoskeletal system, and the environment. With the assistance of computational tools such as MapleSim [1], AnyBody [2], and OpenSim [3], researchers were able to analyze the kinematic and kinetic properties of different locomotion tasks using detailed musculoskeletal models. Assuming natural movement is the result of some optimization done by CNS [4], researchers have simulated realistic movement such as walking [5]–[8], running [9], and pathological gait [10]–[12] using predictive simulation (i.e., a simulation platform capable of predicting movement based on the system dynamics and task requirements without experimental reference).

Manuscript received: February 18, 2023; Revised: May 13, 2023; Accepted: June 5, 2023. This paper was recommended for publication by Editor Abderrahmane Kheddar upon evaluation of the Associate Editor and Reviewers' comments. This work was supported in part by NSERC Discovery under Grant RGPIN-2018-04850 and Grant RGPIN2020-05097, John R. Evans Leaders Fund Canadian Foundation for Innovation, the Ontario Research Fund (ORF), and the New Frontiers in Research Fund under Grant NFRFE2018-01698 and Grant NFRFE2022-620.

Jiacheng Weng and Arash Arami are with the Department of Mechanical and Mechatronics Engineering, University of Waterloo, 200 University Ave W, Waterloo, ON N2L 3G1, Canada (e-mail:j5weng@uwaterloo.ca; arash.arami@uwaterloo.ca). Arash Arami is also with Toronto Rehabilitation Institute (KITE), University Health Network, Toronto, ON, Canada. Ehsan Hashemi is with the Mechanical Engineering Department of the University of Alberta (e-mail:ehashemi@ualberta.ca).
Corresponding author: Arash Arami, (arash.arami@uwaterloo.ca).
Digital Object Identifier (DOI): see top of this page.

One common challenge for generating realistic movement using predictive simulation is to obtain the optimal cost function that captures the optimality of the actions in the context of the task. For walking, researchers have proposed cost terms (e.g., muscle activation, motion smoothness, and stability [10], [11], [13], [14]) that effectively contribute to the naturalness of the simulated gait. In most existing work, cost function compositions (i.e., the relative weighting of the cost terms) are manually or heuristically tuned [10], [11], [13], [15] based on the researcher's domain knowledge which is labour intensive.

To automate the cost function tuning process, various inverse optimal control (IOC) methods in the form of bilevel optimization (i.e., an inner-loop optimal control problem for movement optimization coupled with an outer-loop cost function tuning problem) have been developed and applied to different locomotion tasks (e.g., walking [6], [16], walking with robotic transfemoral prosthesis [17], and sprinting [18]). However, IOC for locomotion is often difficult to solve due to computationally-expensive inner-loop optimal control problems and inefficient outer-loop cost function weight update methods which are often derivative-free. Although cost function tuning for multiple subjects has been performed with torque driven humanoid models [16], multi-subject cost function tuning with musculoskeletal models (which is more complex than humanoid models due to muscle activation dynamics and redundancy) has been remained a challenge. Recently, Weng *et al.* developed the Adaptive Reference Inverse Optimal Control (AR-IOC) [7] for musculoskeletal walking which used a gradient-based optimization in its outer-loop cost function tuning. This results in a drastic reduction of computational time when compared to derivative-free methods used before. Such improvement enables researchers to investigate interesting questions that have never been attempted before in the IOC setting: for instance, how does the CNS cost function varies with respect to the walking speed? To answer this question, in this paper, we solve a large collection of IOC problems using the AR-IOC algorithm [7] based on reference data collected at different walking speeds. The main contributions of this paper include:

- identifying the optimal cost functions for 5 subjects under 4 different walking speeds
- investigating the relationship between cost function composition and the walking speeds

II. Methods

In this section, we first describe the gait data collection procedures, followed by musculoskeletal model formulation

IEEE Robotics and Automation Letters (RA-L) paper, presented at ICRA 2024, Yokohama, Japan. Cite as RA-L paper.

IEEE Robotics and Automation Letters (RA-L) paper, presented at ICRA 2024, Yokohama, Japan. Cite as RA-L paper.

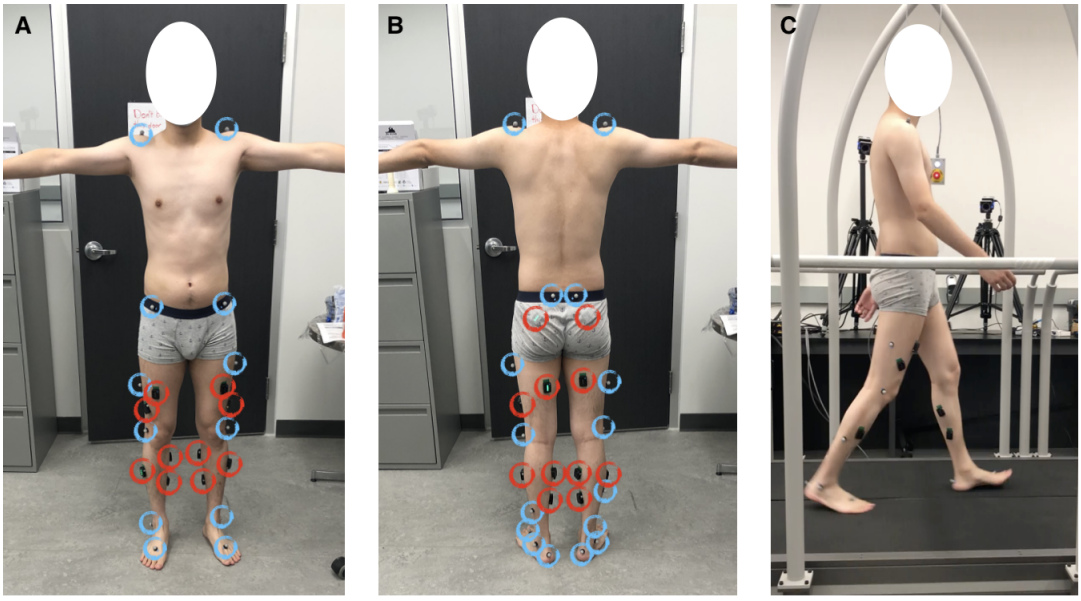

Fig. 1. Sensor and marker placement for walking data collection; A,B) EMG sensor (circled in red) and marker (circled in blue) placement; C) a typical participant walking on the instrumented treadmill at different speeds.

TABLE I
EXPERIMENTAL SETUP DURING THE DATA COLLECTION PHASE

Trial	scaled speed	stride length	walking time (min)	rest time (min)
1	0.2	normal	6	0.5
3	0.3	normal	3	0.5
5	0.4	normal	3	0.5
7	0.5	normal	3	0.5

TABLE II
SUBJECT INFORMATION FOR GAIT DATA COLLECTION

subject	gender	Height (m)	Mass (kg)	Leg length (m)
1	male	1.80	65.73	0.97
2	female	1.69	65.51	0.89
3	male	1.79	106.95	0.93
4	male	1.83	87.80	0.94
5	female	1.61	58.83	0.84

and scaling. Finally, the IOC method for recovering the optimal cost function is detailed.

A. Data Collection

We first collected a dataset of human walking at different speeds. Five able-bodied participants (2 female and 3 male, age 28 ± 3 y/o, height 1.74 ± 0.09 m, weight 77.0 ± 20.0 kg) with no known musculoskeletal injury or motor impairment were recruited and provided written consent prior to participating to the study. The experiment procedures and protocol were approved by the University of Waterloo Clinical Research Ethics Committee (ORE#41794) on April 5, 2022, and conformed with the Declaration of Helsinki. During the experiment, body kinematics, ground reaction forces (GRF), and electromyography (EMG) data are collected synchronously using the Vicon Vero motion capture system (total of eight cameras sampled at 100Hz), Bertec split-belt instrumented treadmill (sampled at 1000Hz), and Delsys EMG sensor system (sampled at 2000Hz), respectively. All signals are upsampled to 2000Hz using linear interpolation for later gait sectioning. Fig. 1 shows an example of the marker and EMG sensor placement on the human body. The marker placement is modified based on the Plugin-gait lower limb convention (Vicon, UK) with sixteen lower-limb markers. Four pelvis markers are placed over the anterior and posterior superior iliac spine. Four markers are placed over the thigh and shank. Two knee markers are placed on the lateral epicondyle. Two ankle markers are placed on the lateral malleolus. Four foot markers are placed on the calcaneous and the second metatarsal head (MH). Two additional shoulder markers on top of the Acromio-clavicular joint are included for torso orientation tracking. Fourteen EMG sensors are placed on major lower-limb muscles for sagittal plane motion (i.e., Gluteus Maximus, Rectus Femoris, Biceps Femoris, Vastus Lateralis, Tibialis Anterior, Soleus, and Gastrocnemius Medialis) to record muscle activities. The exact sensor locations and orientations follow the conventions explained in the Surface Electromyography for the Non-Invasive Assessment of Muscles (SENIAM) project [19].

The experiment comprises two phases: the calibration phase and data collection phase. During the calibration phase, the participant is instructed to stand upright on the treadmill. The marker and GRF data is collected to be used as the reference of the participant's body geometries and weight. A squat-to-toe-standing motion is performed to set the reference for maximum voluntary muscle contraction. During the data collection phase, each participant is instructed to walk barefoot on the treadmill at four different conditions that cover walking with normal strides at four different speeds (summarized in Table I). The walking speed is represented in the scaled form [20]

IEEE Robotics and Automation Letters (RA-L) paper, presented at ICRA 2024, Yokohama, Japan. Cite as RA-L paper.

$$v = \hat{v} \times \sqrt{l_{leg} g} \tag{1}$$

to account for different body geometries, where $v, \hat{v}$ are the actual and scaled speed, respectively, l_{leg} is the leg length, and g is $9.81 m/s^2$. The trials with slower speeds are performed first to avoid sweat accumulation that can influence the accuracy of the EMG measurement. The stride length is self-selected by the participants at their most comfortable gait. The first trial has 6 minutes of walking (4-min acclimatization and 2-min data collection) for proper adaptation to the treadmill walking according to [21]. In the later trials, we reduce the walking time to 3 minutes (1-min acclimatization and 2-min data collection) to reduce the overall experimental time to avoid muscle fatigue. For each trial, two-minute walking data is used for processing. Between each trial, half a minute break is given for the participants to rest. The participant's gender, height, leg length, and mass are summarized in Table II. The actual walking speed for each participant can be calculated using (1).

The collected marker and GRF data require pre-processing before being used in the IOC analysis. The pipeline for data analysis is summarized and shown in the top portion of Fig. 3. First, Savitzky-Golay filters [22] are used on the upsampled marker and GRF data (at 2000Hz) to reduce noise. Then, individual gait data is split into gait cycles by identifying heel strikes using the smoothed vertical GRF data with the threshold of 50 N. Then, the individual gait trajectories are interpolated to a fixed length. Finally, the interpolated data is averaged to one single gait trajectory and formatted to be used in the OpenSim environment. The resolution of the averaged gait (1000 points for half a gait cycle) is sufficient for the study because it is already higher than the discretization of the direct collocation problem (15 points for half a gait cycle). The sectioned EMG signals are further processed to be compared with the muscle excitation signals obtained from the IOC analysis to ensure the validity of our simulations.

B. Musculoskeletal Models

Prior to solving the IOC problems, the subject-specific musculoskeletal models are constructed (shown as the *OpenSim model scaling* block in Fig. 3). The baseline musculoskeletal model that is used for scaling is modified based on the *gait10dof18musc* model provided by OpenSim [3]. This modified model (shown in Fig. 2) allows sagittal-plane (2D) motion with 12 degrees of freedom (DoF), including 9 DoFs at local joints (hip, knee, ankle, metatarsophalangeal (toe), and torso), 3 DoFs for global movement. Actuators include 1 torso torque actuator with 200Nm of maximum torque and 18 Lower limb muscles (Hamstrings HAM, Biceps Femoris short head BFsh, Gluteus Maximus GM, Iliopsoas IL, Rectus Femoris RF, Vasti VA, Gastrocnemius GC, Soleus SOL, and Tibialis Anterior TA). The addition of the torso torque actuator comparing to [7] is for more natural pelvis movement and improved lower limb gait trajectoies. Passive joint torque actuators with double exponent formulation [23] are added to hip, knee, and ankle joints to simulate the effect of ligaments.

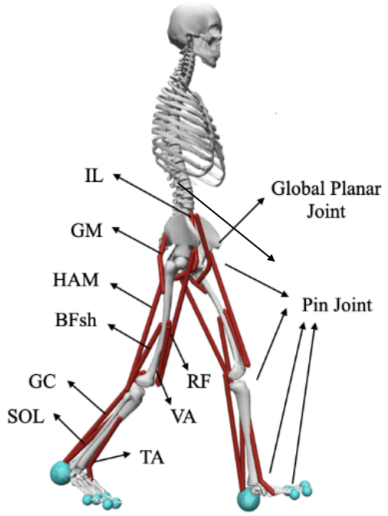

Fig. 2. The musculoskeletal model has 12 DoFs, 18 lower-limb muscles, and 1 ideal torque actuator at torso.

The metatarsophalangeal joints are passively actuated using linear passive spring-damper actuators. The default muscle fibre lengths and pennation angles are obtained from [24]. The default tendon slack lengths are obtained from [25]. Six Hunt Crossley contact spheres at the heel, first MH, third MH, fifth MH, hallux, and middle toe are added for each foot to cover all high-pressure zones during walking [26].

The subject-specific musculoskeletal models are scaled from the baseline model using the same methods explained in [7]. The body segment sizes, mass, contact sphere locations, optimal muscle fibre lengths, and maximum isometric muscle force are scaled during the process to ensure accurate estimation of the participant's body geometries and muscle strengths.

C. Optimization Approach

The pipeline for solving the IOC problem is shown at the bottom portion of Fig. 3. Prior to solving the IOC problems, the experimentally obtained data, detailed in section II-A, is further processed to ensure proper dynamic feasibility in the simulation. First, inverse kinematics is performed to recover the coordinate trajectories by using the experimentally obtained marker data along with the scaled musculoskeletal models from section II-B. Then, the inverse kinematic results and the experimentally obtained GRF data are used to solve a predictive simulation problem (formulated using direct collocation) with kinematic and ground reaction force tracking. The tracking results are then used as the reference trajectories in the IOC problems.

For cost function weight tuning, we use the previously developed AR-IOC approach that incorporates efficient inner-loop gait optimization using direct collocation and gradient-based weight updates in the outer loop [7]. The inner-loop direct collocation problems optimize the gait by minimizing a composite cost function with similarities to our previous work [7] as shown below:

IEEE Robotics and Automation Letters (RA-L) paper, presented at ICRA 2024, Yokohama, Japan. Cite as RA-L paper.

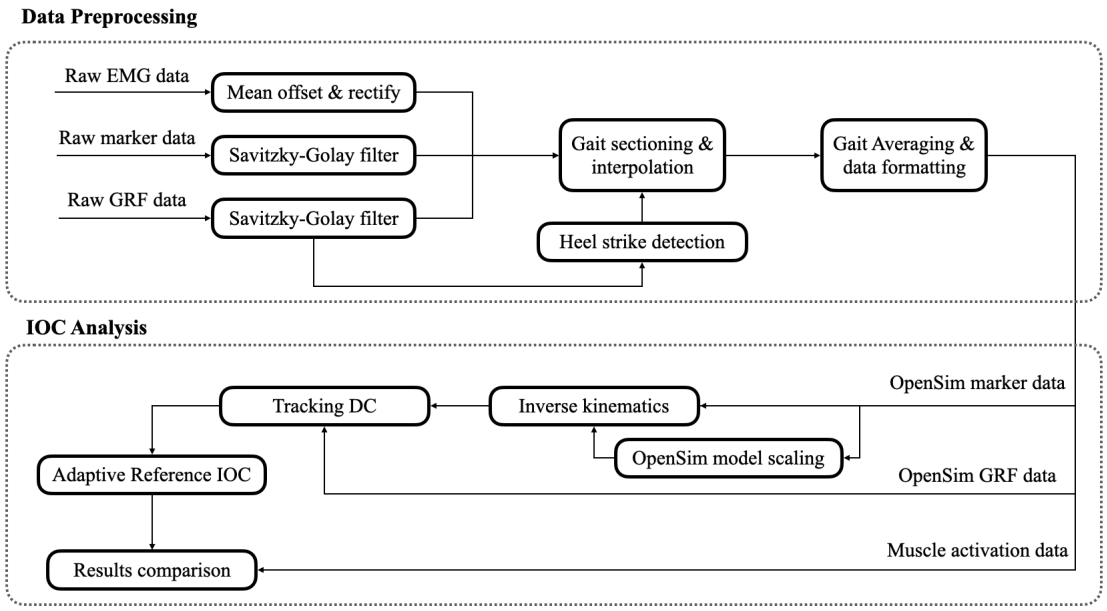

Fig. 3. The pipeline of walking data analysis from data preprocessing to IOC. The raw EMG, marker, and GRF data were sampled at 2000Hz, 100Hz, and 1000Hz respectively. The marker and GRF data are first oversampled to 2000Hz using linear interpolation to best maintain the EMG information. All data is then sectioned into individual gaits based on the heel strikes. The sectioned gaits are then interpolated to the same length, and averaged to be used for the IOC analysis.

$$
\begin{aligned}
J =& \frac{1}{d}\int_0^{t_f} (\boldsymbol{\omega}^T \boldsymbol{C}) dt \\
=& \frac{1}{d}\int_0^{t_f} \Bigg[10 \sum_i \left(\frac{u_i^3}{n}\right) + 10^{-2} \sum_j \hat{\tau}_j^2 \\
&+ \omega_{torso} \times 10^{10} (\hat{\tau}_{torso})^2 \\
&+ \omega_{CoM} \times (\hat{a}_{CoM})^2 \\
&+ \omega_{slide} \times 10^2 \left[\left(\hat{F}_{lf}^y \hat{v}_{lf}^{fx}\right)^2 + \left(\hat{F}_{rf}^y \hat{v}_{rf}^{fx}\right)^2 \right] \\
&+ \omega_{stability} \times 10 (\hat{p}_{CoMx} - \hat{p}_{midBoS})^2 \Bigg] dt. \qquad (2)
\end{aligned}
$$

This cost function includes six cost terms and four tunable weights. No tunable weight is considered for the first two cost terms. Fixing the first weight is to avoid trivial weight vector scaling. Fixing the second weight is to improve the IOC stability by preventing direct collocation solutions from jumping between normal walking and abnormal walking with excessive use of passive joint torque [7]. Such jumps only occur when the weight of the second term is within a narrow band. Thus, as a trade off, we fix that weight far away from mentioned narrow band to ensure AR-IOC stability. Fortunately, the effect of this trade off on optimality of the obtained cost function is small as changing the second weight when it is far away from that sensitive band has small impact to the optimized gait. Physical quantities (e.g., torque τ, force F, velocity v, and position p) are scaled to their dimensionless form as detailed in [7].

The first term of the composite cost function penalizes the sum of cubed muscle excitation u divided by the total number of muscles n where i is the muscle index. The second term penalizes the squared passive ligament torque $\hat{\tau}_j$ to prevent the excessive use of ligaments (that can result in joint hyperextension, joint damage and pain), where j is the passive joint actuator index at hip, knee, and ankle joints. The third term penalizes the squared torso torque $\hat{\tau}_{torso}$ which is the torque in Nm applied between lumbar and pelvis. This term replaces the torso angle term in the previous study [7] to provide a more universal approach for achieving good upper body posture and removes the dependencies on upper body tracking and torso calibration of the musculoskeletal models. Note that the coefficient in front of this term is large as the optimized torque values between lumbar and pelvis is small. This is because the musculoskeletal model in this study assumes a rigid upper body where small torque is enough to balance the torso during gait. This is considered as one of the limitations of our study which will be discussed at the end of section III. The fourth term penalizes the squared center of mass (CoM) acceleration which improves the knee flexion during stance as well as optimization stability. The fifth term penalizes the squared foot sliding as a product of the vertical ground reaction force (GRF) $\hat{F}^y$ and the horizontal foot velocity $\hat{v}^{fx}$, where lf, rf represent left and right feet. This term helps reduce excessive foot dragging behaviour in simulation at fast walking speeds. The last term encourages stability and knee extension during swing by penalizing the squared deviation of the CoM position $\hat{p}_{CoMx}$ from the center of the base of support (BoS) $\hat{p}_{midBoS}$ along the forward direction. Coefficients of the cost terms scale the cost values to the same order of magnitude given the desired motion trajectories from the experiment. Finally, the integrated cost is divided by the total distance travelled d measured at the CoM to avoid undesired optimized gait trajectories such as extremely short steps. Note that each cost term was included

IEEE Robotics and Automation Letters (RA-L) paper, presented at ICRA 2024, Yokohama, Japan. Cite as RA-L paper.

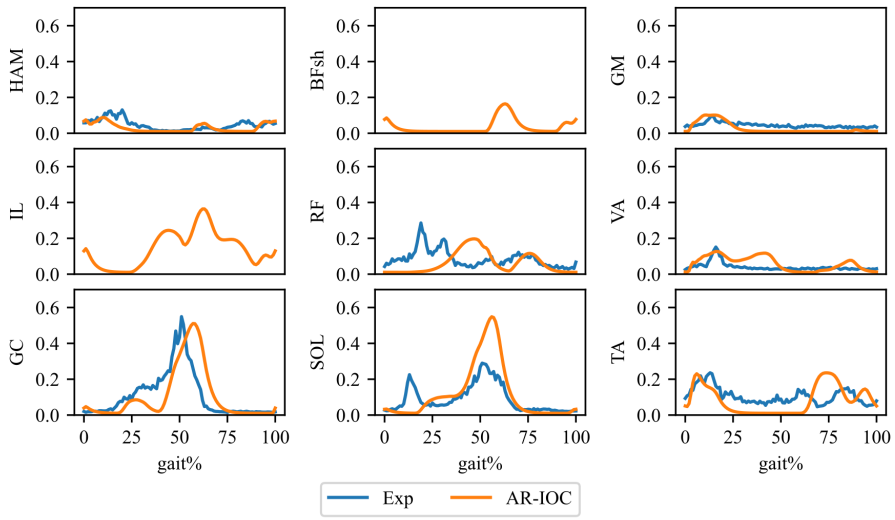

Fig. 4. Sample comparison between the scaled experimental EMG signals and the muscle excitation signals from AR-IOC over a full gait cycle. Data is from a representative participant walking at 0.91m/s. EMG signals for BFsh and IL are not available as these two muscles are difficult to measure with surface EMG sensors.

in our cost function as it improves the obtained gait. Cost terms with similar effects on gait improvement (i.e., redundant cost terms) or with no improvement are avoided.

For outer-loop weight update, we use the previously developed AR-IOC algorithm. AR-IOC performs gradient-based weight updates by comparing the unweighted cost values between the optimized and the reference trajectories. The details of AR-IOC algorithm is provided in [7].

III. Results and Discussion

To study the relationship between the optimal cost weights and the walking speed, a total of 20 IOC problems (i.e., five subjects walking at four different speeds) are solved using the AR-IOC algorithm. The resultant gait patterns from all problems closely resemble the experimental observations with joint angle errors of 3.1 $\pm$ 2.2 deg, 3.2 $\pm$ 2.3 deg, and 2.3 $\pm$ 1.9 deg, and average Pearson correlation of 0.99, 0.99, and 0.99 at hip, knee, and ankle, respectively. The GRFs also match with experimental data closely with errors of 27.2 $\pm$ 24.7 N and 9.9 $\pm$ 11.3 N, and average Pearson correlation of 0.99 and 0.97 along vertical and horizontal directions, respectively.

Fig. 4 provides a sample comparison between the experimental EMG signals from a representative participant walking at 0.91 m/s and the muscle excitation signals obtained from the AR-IOC solution. The magnitude of the EMG signals are scaled to match the muscle excitation for visualization purposes. Note that BFsh and IL do not have EMG comparisons because these two muscles could not be measured by our surface EMG sensors. The comparison shows a close match in the overall shape of the muscle excitation patterns. However, due to the limitation of the surface EMG measurement (e.g., placement accuracy, contact quality, and EMG crosstalk) and the 2D simulation without lateral movement, there are still some minor differences such as the missing initial peaks for SOL and RF muscles. Fig. 5 illustrates the kinematic and GRFs variation for the same participant along with the optimized gait trajectories from AR-IOC. It also illustrates how the converged composite cost weights vary with respect to the gait speed.

The values of the final cost weights under different walking speeds for all participants are summarized in Fig. 6. As the experimental data, the musculoskeletal model, and the cost function differ from our previous study [7], the optimized weights differ from those obtained before. However, the previously obtained weights for three common cost terms did align with the new findings in this study. Given participants' scaled walking speed between 0.3 and 0.4, ω_{CoM} (0.61$\pm$0.33), ω_{slide} (1.18$\pm$0.46), and $\omega_{stability}$ (0.34$\pm$0.18) from [7] all lie within the range of the newly obtained results in Fig. 6. Fig. 6A, D suggests that the CNS significantly increases the CoM acceleration weights and the stability weights to maintain gait at a higher speed. Moreover, the foot sliding weights shown in Fig. 6B reduce when the walking speed increases while the torso effort weights in Fig. 6C show no significant changes. The linear function describing how CNS alters the weights as well as their p values for the F-test (i.e., tested against a constant model with no trends) are shown below:

$$\omega_{torso} = 6.53 + 5.97\hat{v}, \qquad p > 0.05, \tag{3}$$
$$\omega_{CoM} = -0.63 + 4.89\hat{v}, \qquad p < 0.05, \tag{4}$$
$$\omega_{slide} = 5.81 - 11.89\hat{v}, \qquad p < 0.05, \tag{5}$$
$$\omega_{stability} = -0.35 + 2.26\hat{v}, \qquad p < 0.05. \tag{6}$$

The negative constant terms for ω_{CoM} and $\omega_{stability}$ are caused by fitting the linear trends. The actual weights are all non-negative.

The Pearson correlation between the final (converged) weight values for all participants (i.e., ω_{CoM}, ω_{slide}, ω_{torso}, and $\omega_{stability}$) and the scaled walking speed $\hat{v}$ and the scaled stride time $\hat{t}_s$ are summarized in Table III, where

IEEE Robotics and Automation Letters (RA-L) paper, presented at ICRA 2024, Yokohama, Japan. Cite as RA-L paper.

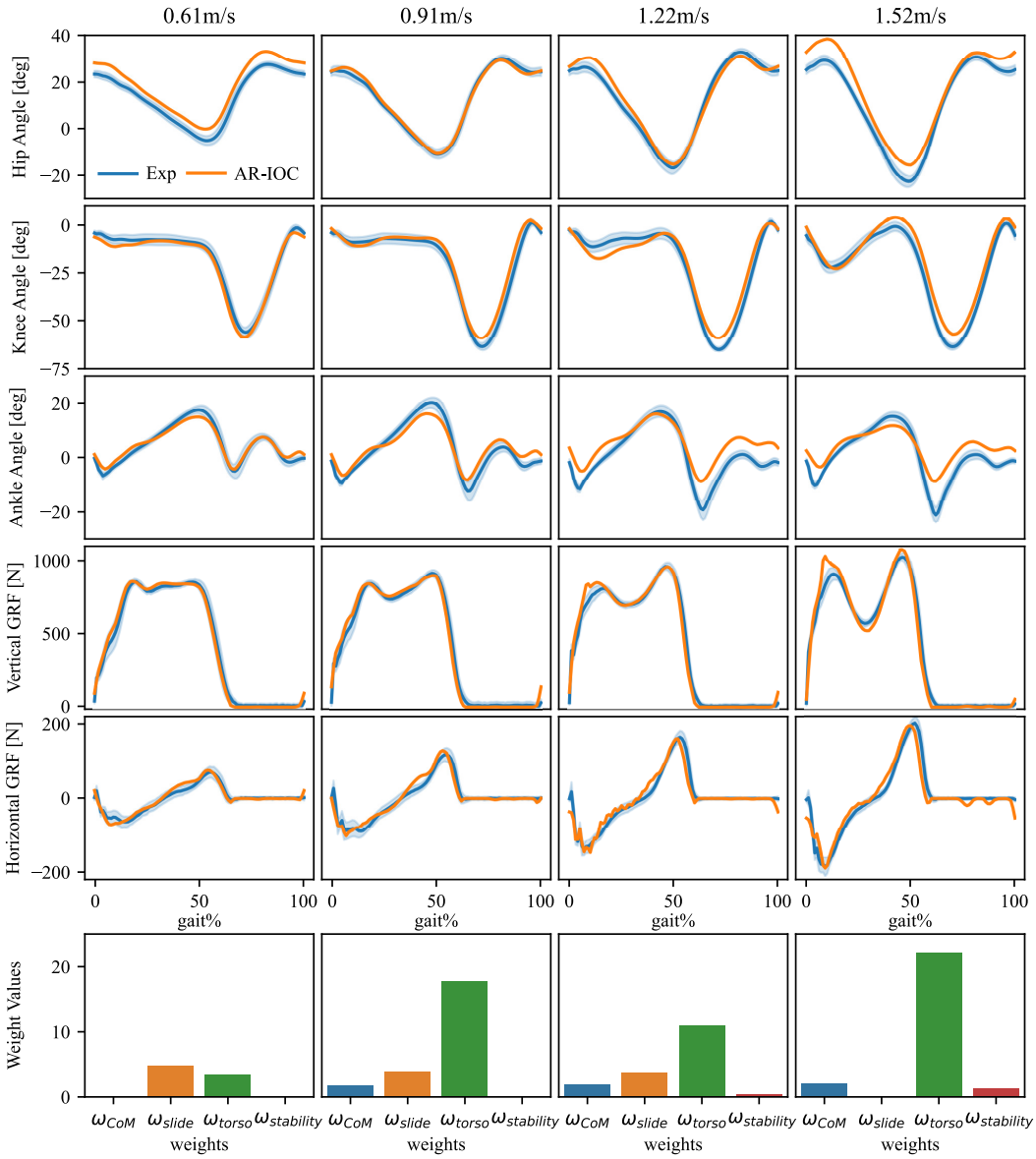

Fig. 5. Comparison between the experimental gait (mean $\pm$ standard deviation SD) and the optimized gait for a representative participant in normal walking condition over four walking speeds. The corresponding optimal weight values are included at the bottom row which shows increasing trends for ω_{CoM}, ω_{torso}, $\omega_{stability}$, and a decreasing trend for ω_{slide} with respect to walking speeds.

TABLE III
PEARSON CORRELATION COEFFICIENTS BETWEEN SCALED WALKING PARAMETERS AND COST WEIGHTS FOR FIVE SUBJECTS WALKING WITH NORMAL STRIDE LENGTHS.

	$\hat{v}$	$\hat{t}_s$	ω_{CoM}	ω_{slide}	$\omega_{torso_{ef}}$	$\omega_{stability}$
$\hat{v}$	1	-0.90	0.57	-0.75	-0.03	0.53
$\hat{t}_s$	-0.90	1	-0.44	0.75	0.046	-0.41

$\hat{t}_s = t_s/\sqrt{l_{leg}/g}$. As the scaled walking speed alone cannot fully describe the walking condition, we also included scaled stride time for a more comprehensive correlation analysis. The torso effort weight ω_{torso} shows relatively small correlations to the walking speed and stride time. As the muscle excitation cost term does not have tunable weights in (2), it may indicate that CNS has not significantly shifted the effort minimization between the lower and the upper bodies across different speeds and stride duration. The foot sliding weight ω_{slide} exhibits a large negative correlation with the scaled velocity. This behaviour aligns with the experimental observation that participants' feet slid against the treadmill during swing more often at higher walking speeds. As the walking speed increases, larger steps are required which reduces the height of the CoM during walking. To maintain ground clearance during foot swing, more knee flexion is required which is against the muscle excitation cost term. As a result, CNS reduces the foot sliding weight and tolerate more foot sliding during the swing phase. Finally, both the CoM acceleration weight ω_{CoM} and the stability weight $\omega_{stability}$ have positive correlations with the scaled walking speed. This indicates an increased attention to increase overall motion smoothness and stability to combat the unavoidable increase in muscle excitation at

IEEE Robotics and Automation Letters (RA-L) paper, presented at ICRA 2024, Yokohama, Japan. Cite as RA-L paper.

IEEE Robotics and Automation Letters (RA-L) paper, presented at ICRA 2024, Yokohama, Japan. Cite as RA-L paper.

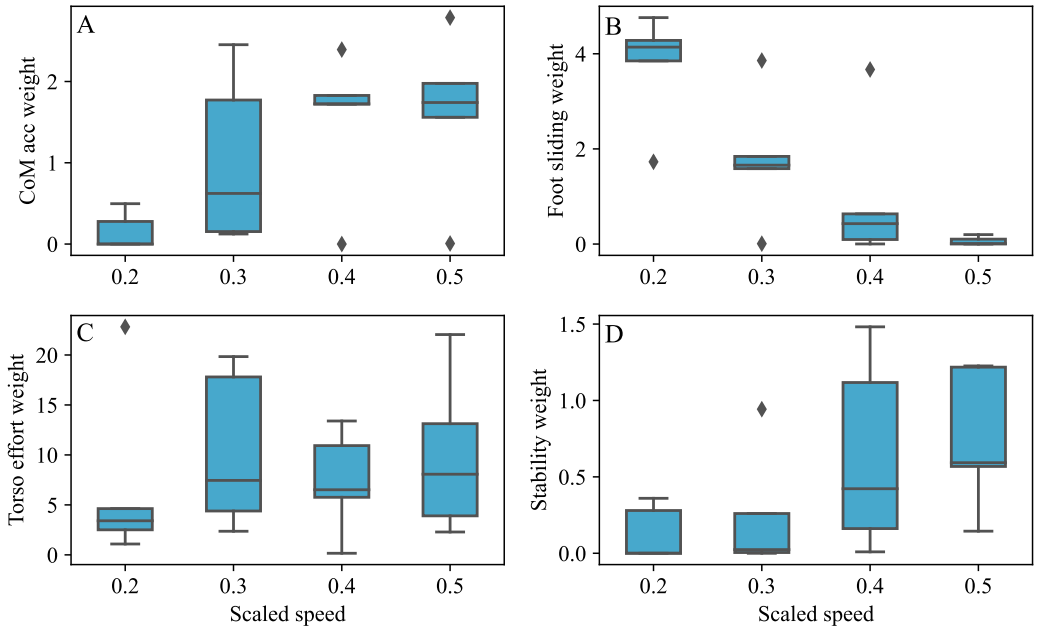

Fig. 6. Comparison between cost weights and scaled walking speed including all participants. At a faster walking speed, in A and D suggest increases in the CoM acceleration and the stability weights; B suggests a decrease in the foot sliding weights; and C shows no significant changes to the torso effort weights.

higher walking speeds. In addition, there is an alternative way of interpreting such correlations. As the muscle excitation cost term is fixed in (2), increases in other weights (i.e., ω_{CoM} and $\omega_{stability}$) indicate an equivalent reduction in the weight of muscle excitation. This aligns with the intuition as more energy is required for faster walking, and consequently a reduction in weights for the energy-related terms (i.e., the muscle excitation term and the torso effort term) is required.

There are some limitations to this study. First, the musculoskeletal model oversimplified the upper body which may not be capable of representing the proper energy expenditure (including the effort due to other segments motion and muscle co-contraction). Including arms and muscle actuators will allow more accurate torso effort calculation. The constraints of Saggital plane movement may also limit the energy calculation. In addition, a possible limitation of using IOC to unveil how CNS controls our movement is the lack of inclusion of the right cost terms. For example, the cost terms in this study may only capture a projection of a true and more complex CNS cost function which may not generalize to other locomotion tasks.

A possible challenge of using the IOC methods in finding the correlation between the cost weights to the walking tasks is the presence of the redundant cost terms. Having redundant cost terms allows obtaining optimal behaviour with different cost weights. This will also affect the convergence of the IOC methods, including AR-IOC. We prevent this issue by carefully designing our cost function composition. However, the cost function design will require more effort for other less-studied movement or locomotion tasks due to the complex interaction between the cost terms, cost weights, and the musculoskeletal system.

Furthermore, different anthropometric parameters, such as body geometries, and participants weight may have an effect on the optimal cost weights. However, the current sample size is not sufficient for investigating such correlations. The study on those correlations require a much larger dataset and will be addressed in the future work.

IV. Conclusion and Future Work

Utilizing an optimal control framework, this study investigated how the central nervous system alters the weights of a composite cost function to maintain stable walking at different speeds. A correlation analysis between the optimal cost function weights and the walking speeds has been conducted. Walking data at four walking speeds conditions were collected from five able-bodied individuals. The collected data was used to recover the optimal cost functions by solving 20 inverse optimal control problems using a computationally efficient adaptive reference inverse optimal control algorithm [7]. The converged cost function weights suggest that CNS reduces the weights for foot sliding, muscle excitation, and torso effort when walking speed increases. We observed no significant shift in effort reduction weighting between the upper and the lower body as a function of walking speed. However, the simplified musculoskeletal model used in this study excluded upper limb segments such as arms and hands which may reduce the accuracy of the upper limb effort calculation. In future studies, a full-body musculoskeletal model along with full-body motion tracking will be used to investigate how the CNS alters the optimal weights in more diverse conditions, e.g. sprinting, running, walking when lower limb muscles are fatigued. EMG signals can be included as a part of the AR-IOC formulation in the future work. Furthermore, more participant data can be collected to further investigate the correlation between the optimal cost weights and other anthropometric factors such as body geometries and weights.

REFERENCES

[1] M. Sharif Shourijeh and J. McPhee, "Forward dynamic optimization of human gait simulations: a global parameterization approach," *Journal of Computational and Nonlinear Dynamics*, vol. 9, no. 3, 2014.

[2] M. Damsgaard, J. Rasmussen, S. T. Christensen, E. Surma, and M. De Zee, "Analysis of musculoskeletal systems in the anybody modeling system," *Simulation Modelling Practice and Theory*, vol. 14, no. 8, pp. 1100–1111, 2006.

[3] S. L. Delp, F. C. Anderson, A. S. Arnold, P. Loan, A. Habib, C. T. John, E. Guendelman, and D. G. Thelen, "Opensim: open-source software to create and analyze dynamic simulations of movement," *IEEE transactions on biomedical engineering*, vol. 54, no. 11, pp. 1940–1950, 2007.

[4] E. Todorov and M. I. Jordan, "Optimal feedback control as a theory of motor coordination," *Nature neuroscience*, vol. 5, no. 11, pp. 1226–1235, 2002.

[5] T. W. Dorn, J. M. Wang, J. L. Hicks, and S. L. Delp, "Predictive simulation generates human adaptations during loaded and inclined walking," *PloS one*, vol. 10, no. 4, p. e0121407, 2015.

[6] V. Q. Nguyen, R. T. Johnson, F. C. Sup, and B. R. Umberger, "Bilevel optimization for cost function determination in dynamic simulation of human gait," *IEEE Transactions on Neural Systems and Rehabilitation Engineering*, vol. 27, no. 7, pp. 1426–1435, 2019.

[7] J. Weng, E. Hashemi, and A. Arami, "Adaptive reference inverse optimal control for natural walking with musculoskeletal models," *IEEE Transactions on Neural Systems and Rehabilitation Engineering*, vol. 30, pp. 1567–1575, 2022.

[8] M. L. Felis and K. Mombaur, "Using optimal control methods to generate human walking motions," in *International Conference on Motion in Games*. Springer, 2012, pp. 197–207.

[9] A. J. Van den Bogert, M. Hupperets, H. Schlarb, and B. Krabbe, "Predictive musculoskeletal simulation using optimal control: effects of added limb mass on energy cost and kinematics of walking and running," *Proceedings of the Institution of Mechanical Engineers, Part P: Journal of Sports Engineering and Technology*, vol. 226, no. 2, pp. 123–133, 2012.

[10] A. Falisse, G. Serrancolí, C. L. Dembia, J. Gillis, I. Jonkers, and F. De Groote, "Rapid predictive simulations with complex musculoskeletal models suggest that diverse healthy and pathological human gaits can emerge from similar control strategies," *Journal of The Royal Society Interface*, vol. 16, no. 157, p. 20190402, 2019.

[11] A. Falisse, L. Pitto, H. Kainz, H. Hoang, M. Wesseling, S. Van Rossom, E. Papageorgiou, L. Bar-On, A. Hallemans, K. Desloovere *et al.*, "Physics-based simulations to predict the differential effects of motor control and musculoskeletal deficits on gait dysfunction in cerebral palsy: a retrospective case study," *Frontiers in human neuroscience*, vol. 14, p. 40, 2020.

[12] M. Shushtari, R. Nasiri, and A. Arami, "Online reference trajectory adaptation: A personalized control strategy for lower limb exoskeletons," *IEEE Robotics and Automation Letters*, vol. 7, no. 1, pp. 128–134, 2021.

[13] B. R. Umberger, "Stance and swing phase costs in human walking," *Journal of the Royal Society Interface*, vol. 7, no. 50, pp. 1329–1340, 2010.

[14] M. Ackermann and A. J. Van den Bogert, "Optimality principles for model-based prediction of human gait," *Journal of biomechanics*, vol. 43, no. 6, pp. 1055–1060, 2010.

[15] J. Weng, E. Hashemi, and A. Arami, "Natural walking with musculoskeletal models using deep reinforcement learning," *IEEE Robotics and Automation Letters*, vol. 6, no. 2, pp. 4156–4162, 2021.

[16] D. Clever, R. M. Schemschat, M. L. Felis, and K. Mombaur, "Inverse optimal control based identification of optimality criteria in whole-body human walking on level ground," in *2016 6th IEEE International Conference on Biomedical Robotics and Biomechatronics (BioRob)*. IEEE, 2016, pp. 1192–1199.

[17] W. Liu, J. Zhong, R. Wu, B. L. Fylstra, J. Si, and H. H. Huang, "Inferring human-robot performance objectives during locomotion using inverse reinforcement learning and inverse optimal control," *IEEE Robotics and Automation Letters*, vol. 7, no. 2, pp. 2549–2556, 2022.

[18] A. L. E. N. Kleesattel and K. Mombaur, "Inverse optimal control based enhancement of sprinting motion analysis with and without running-specific prostheses," in *2018 7th IEEE International Conference on Biomedical Robotics and Biomechatronics (Biorob)*. IEEE, 2018, pp. 556–562.

[19] H. J. Hermens, B. Freriks, R. Merletti, D. Stegeman, J. Blok, G. Rau, C. Disselhorst-Klug, and G. Hägg, "European recommendations for surface electromyography," *Roessingh research and development*, vol. 8, no. 2, pp. 13–54, 1999.

[20] A. L. Hof, "Scaling gait data to body size," *Gait & posture*, vol. 3, no. 4, pp. 222–223, 1996.

[21] C. Meyer, T. Killeen, C. S. Easthope, A. Curt, M. Bolliger, M. Linnebank, B. Zörner, and L. Filli, "Familiarization with treadmill walking: How much is enough?" *Scientific reports*, vol. 9, no. 1, pp. 1–10, 2019.

[22] A. Savitzky and M. J. Golay, "Smoothing and differentiation of data by simplified least squares procedures." *Analytical chemistry*, vol. 36, no. 8, pp. 1627–1639, 1964.

[23] F. C. Anderson and M. G. Pandy, "Dynamic optimization of human walking," *J. Biomech. Eng.*, vol. 123, no. 5, pp. 381–390, 2001.

[24] S. R. Ward, C. M. Eng, L. H. Smallwood, and R. L. Lieber, "Are current measurements of lower extremity muscle architecture accurate?" *Clinical orthopaedics and related research*, vol. 467, no. 4, pp. 1074–1082, 2009.

[25] V. Nguyen, "Predictive simulation of human movement and applications to assistive device design and control," *Doctoral Dissertations, 1803, UMassAmherst, MA, US*, 2019.

[26] T. C. Pataky and J. Y. Goulermas, "Pedobarographic statistical parametric mapping (pspm): a pixel-level approach to foot pressure image analysis," *Journal of biomechanics*, vol. 41, no. 10, pp. 2136–2143, 2008.

IEEE Robotics and Automation Letters (RA-L) paper, presented at ICRA 2024, Yokohama, Japan. Cite as RA-L paper.